Microstructure and mechanical behavior of cross-linked biopolymer networks

Zagar, Goran

Chapter 4

Rigidly cross-linked networks: Small strain behavior

Based on: G. Žagar, P.R. Onck and E. Van der Giessen, "*Small strain topological effects of biopolymer networks with rigid cross-links*", In IUTAM Symposium on Cellular, Molecular and Tissue Mechanics, Eds. K. Garikipati and E.M. Arruda, pp. 161-169, (2010)

The scientific interest in the mechanics of filamentous bipolymer networks is extensive (Kasza et al., 2007). Rheological experiments of various *in vitro* networks showed a strong dependence of the small strain behavior on the filament concentration as well as on concentration of the cross-linking proteins (Janmey et al., 1991; MacKintosh et al., 1995; Gardel et al., 2004a). Theoretical mean field affine deformation models, based on the physics of thermally excited semi-flexible polymers, predict the filament concentration dependence of the initial elastic shear modulus G_0 in the regimes of entangled and densely cross-linked actin gels to be a power law with exponents 11/5 and 5/2, respectively (MacKintosh et al., 1995; Gardel et al., 2004a). On the other hand, mean field models based on the bending of stiff polymers (Kroy and Frey, 1996; Satcher and Dewey, 1996) propose a quadratic filament concentration dependence, which is the dependence commonly used for describing porous materials like foams (Gibson and Ashby, 1997). In addition, a recent theoretical study of discrete three-dimensional (3D) F-actin networks (Huisman et al., 2007) suggests that an increasing connectivity in the network significantly enhances its initial shear modulus. Although intuitive, the dependence of the initial mechanical behavior on network connectivity is generally nontrivial and still poorly understood.

In this chapter we explore the mechanical behavior of networks at small strains

and in the limit of rigid cross-links (RCL). The distribution of coordination over the L, T and X cross-link types of connectivity 2, 3 and 4, respectively (see § 3.1), proves to be very important for the initial shear modulus. After proper scaling of the initial network stiffness, we identify the topological function, $f(\mathcal{T}) = (l_c/\xi)(\tilde{n}_X)^{2.5}$, that describes the dependence of the initial response on network topology in terms of mean section length between cross-links l_c, mesh size ξ and fraction of X cross-links $\tilde{n}_X$.

4.1 Scaling relations

The mechanical properties of biopolymer networks with rigid cross-links are determined by the constituent filaments between the cross-links and by the topology of the network. When the persistence length l_p of the filaments is much larger than the average length of the sections, i.e. $l_p \gg l_c$, the sections can be considered as being straight. In addition, networks are generally expected to be bending dominated for the mean cross-link coordination of being below ≈ 6 (Buxton and Clarke, 2007) and for the ratio of filament bending and stretching stiffness $l_b = \sqrt{\kappa/\mu} \ll l_c$ (Head et al., 2003). An isotropic network with cross-link coordination that is either 2, 3 or 4 made from straight and slender sections ($l_c/l_b \gg 1$) therefore, is a bending dominated structure, for which a scaling relation of the initial modulus can be developed as follows (Gibson and Ashby, 1997; Satcher and Dewey, 1996; Žagar et al., 2010).

Microscopically, the network can be considered as an interconnected collection of *bending beams* of length l with random spatial orientation. The macroscopic strain of the network reflects the microscopic bending of beams characterized by a deflection δ. If the strain at the beam is $\varepsilon = \delta/l$, the macroscopic strain $\langle\varepsilon\rangle$, in principle, is obtained by averaging this beam-level strain over their spatial orientations.

Consider now, for example, that the macroscopic deformation of beams is simple shear. In this case, $\langle\varepsilon\rangle$ is an equivalent for macroscopic shear strain, e.g. Γ. Beams respond to bending as described by their force–deflection law, given by $f \propto (\kappa/l^3)\delta$, or in terms of the beam strain $f \propto (\kappa/l^2)\varepsilon$, where κ is the beam bending stiffness. If there are $(1/\xi)^2$ of beams per unit area, each of them contributing on average to the total shear force, then the macroscopic shear stress T of the network scales as $\mathrm{T} \propto (1/\xi)^2(\kappa/l_c^2)\Gamma$, where l_c is the average length of the beams. The initial elastic shear modulus $G_0 = \mathrm{T}/\Gamma$ of such networks then simply scales as

$$G_0 \propto \frac{\kappa}{l_c^4}\left(\frac{l_c}{\xi}\right)^2 f(\mathcal{T}), \tag{4.1}$$

where $f(\mathcal{T})$ is an as yet unknown function that accounts for the network topology. In addition to l_b, isotropic networks as bending structure are therefore characterized by two length scales: the mean length of the bending elements l_c and by the mesh size parameter ξ that represents the mean spacing of bending elements. Moreover, since the network topology is fully determined by the ratio l_0/l_c (see Chapter 3), via topological function $f(\mathcal{T})$ in the scaling relation (4.1) it is expected that the filament length l_0 will emerge as an additional length scale important for the isotropic network. Note that the scaling given in (4.1) lacks a persistence length factor, l_p/l_c, which is present in scaling, $G \propto \kappa/l_c^4 \cdot l_p/l_c \cdot (l_c/\xi)^2$, derived from the force–displacement law of thermally undulated worm-like-chain polymers in the semi-flexible limit (MacKintosh et al., 1995). However, if the beams, that represent filament sections, are considered to be straight ($l_p \gg l_c$) then the dependence on persistence length l_p has to vanishes.

4.2 Numerical simulations and Results

In order to identify an unknown topological function $f(\mathcal{T})$, the scaling relation proposed in (4.1) is investigated numerically.

Sets of seven to ten random realizations of networks — characterized by the triplet (c_f, l_0, l_c) — are systematically generated for initial filament concentration c_f: 1, 1.5, 2 and 2.5mg/ml, filament lengths l_0: 1.5, 1.8 and 2.1μm and several values of the mean section lengths l_c in the range from 0.22 to 0.45μm. The initial elastic shear modulus for each network realization is calculated by subjecting the realization to simple shear in a finite element simulation as described in § 2.3. The material parameters of the filament elements used in the computations are based on F-actin: $\mu = 4 \times 10^{-8}$ N (Liu and Pollack, 2002) for axial stiffness and $\kappa = \omega = 7 \times 10^{-26}$ Nm^2 (Ott et al., 1993) for bending and torsional stiffnesses.

The parameters used for analysing the system are: the mean normalized initial elastic shear modulus $G_0\, l_c^4/\kappa$, the mean geometrical parameter l_c/ξ with mesh size ξ defined in (3.4) and the mean topological parameter $\tilde{n}_X = n_X/n_{cl}$ obtained from expression in (3.2). While $G_0\, l_c^4/\kappa$ and l_c/ξ follow naturally from scaling relation (4.1), the connectivity of the network can be quantified in several equivalent ways, as suggested by the expressions (3.2) and (3.3) in Chapter 3. As the most convenient measure for connectivity, however, we find the fraction of X cross-links $\tilde{n}_X(\tilde{l}_0)$, since it is the slowest varying function of $\tilde{l}_0$ over the entire connectivity range (see Figure 3.2). Obviously, $\tilde{n}_X = 0$ corresponds to an L-only network with connectivity 2, while $\tilde{n}_X = 1$ to an X-only network with connectivity 4.

Figure 4.1a shows the normalized network shear modulus as a function of the

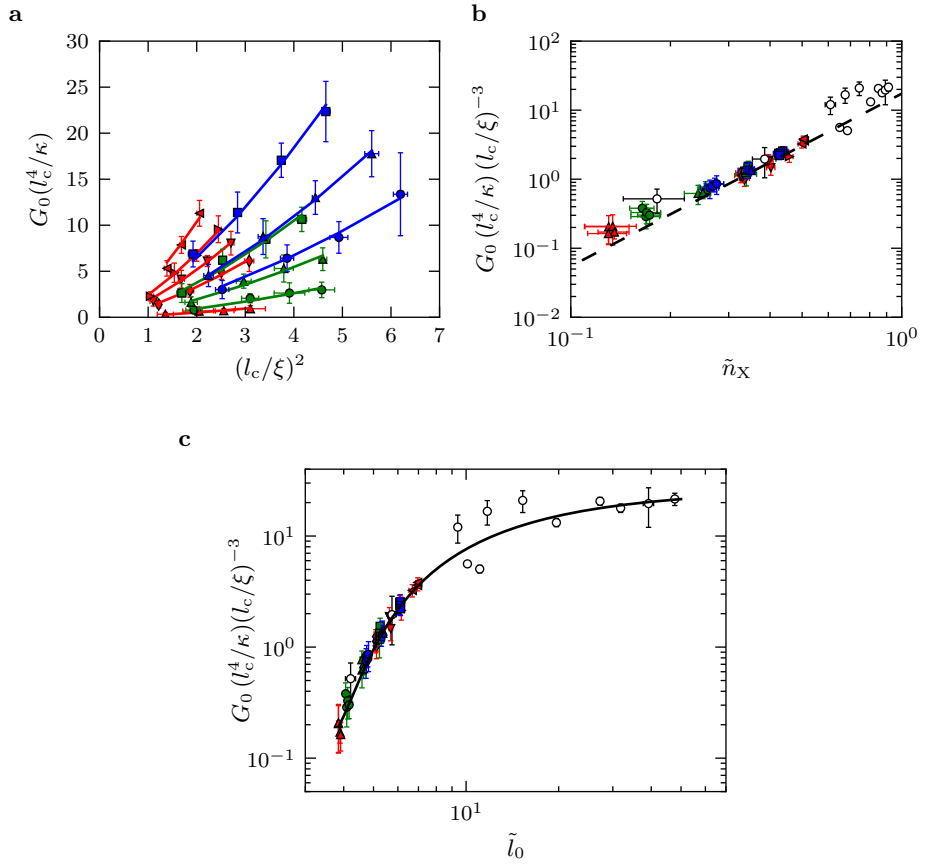

Figure 4.1. Scaling relations. **a**, $G_0 l_c^4/\kappa$ as a function of $(l_c/\xi)^2$ for l_0 [μm]: 1.5 (red), 1.8 (green) and 2.1 (blue) and l_c [μm]: 0.45 (circle), 0.40 (up-triangle), 0.35 (square), 0.30 (diamond), 0.27 (down-triangle), 0.25 (right-triangle) and 0.22 (left-triangle). Lines for constant $\tilde{n}_X$ are a power-law fits with exponent 1.5. By scaling out the dependence on l_c/ξ, the renormalized initial network shear modulus shows a power-law dependence on $\tilde{n}_X$ with exponent 2.5 (dashed line) in **b**, and the dependence on $\tilde{l}_0$ through the function $A[(\tilde{l}_0 - 3)/(\tilde{l}_0 - 1)]^5$ (solid line), with proportionality constant determined by fitting, $A \approx 28 \pm 6$ in **c**. The plots in panel **b** and **c**, in addition to the data of panel **a** (filled symbols) contain the extra (test) data points (open symbols) obtained for various triplets (c_f, l_0, l_c), where c_f ranges from 0.8 to 4 mg/ml; l_0 ranges from 1.5 and 20 μm, and l_c ranges from $\approx 0.02\ l_0$ to $\approx 0.25\ l_0$. The data points in all graphs represent quantities averaged over the set realizations.

geometrical parameter l_c/ξ. Least square fits of all network subsets with constant l_0 and constant l_c indicate a consistent power-law scaling with exponent 3/2. The difference between the curves in Figure 4.1a is clearly due to topological effects, as expected in (4.1). Surprisingly however, from Figure 4.1a follows that the geometrical factor l_c/ξ also enters the topological function $f(\mathcal{T})$.

In order to scale out the influence of l_c/ξ on the shear modulus, the moduli in Figure 4.1a are multiplied with $[(l_c/\xi)^2]^{3/2}$ and the data is re-plotted against the topological parameter $\tilde{n}_X$ in Figure 4.1b. All data sets now collapse onto a single master curve, which furthermore indicates a power-law dependence of the shear modulus G_0 on connectivity $\tilde{n}_X$ with exponent 2.5. The combined results of Figure 4.1a and Figure 4.1b give a complete scaling description of the initial shear modulus of isotropic 3D networks with rigid cross-links as

$$G_0 \propto \frac{\kappa}{l_c^4}\left(\frac{l_c}{\xi}\right)^3 \tilde{n}_X^{2.5}, \tag{4.2}$$

where the network topology function $f(\mathcal{T})$ is identified as

$$f(\mathcal{T}) \propto \frac{l_c}{\xi}\tilde{n}_X^{2.5}. \tag{4.3}$$

In addition, by substituting $\tilde{n}_X$ with expression in (3.2), the scaling relation (4.2) can be rewritten in terms of dependence on $\tilde{l}_0$ as

$$G_0 = A\frac{\kappa}{l_c^4}\left(\frac{l_c}{\xi}\right)^3\left(\frac{\tilde{l}_0-3}{\tilde{l}_0-1}\right)^5. \tag{4.4}$$

Indeed, if now $G_0(l_c^4/\kappa)(l_c/\xi)^{-3}$ is plotted against $\tilde{l}_0$, as shown in Figure 4.1c, all data points follow the trend set by the function, $A[(\tilde{l}_0-3)/(\tilde{l}_0-1)]^5$ where the proportionality factor is determined by fitting, $A \approx 28 \pm 6$.

Thus, the contribution of the network topology to the initial shear modulus G_0 is found to be twofold: firstly, compared to the topology-free scaling law, $G_0 \propto \kappa/l_c^4(l_c/\xi)^2$, there is an extra dependence of G_0 on the ratio l_c/ξ, and secondly, there is a power-law dependence on $\tilde{n}_X$ with exponent 2.5. The network connectivity, here associated to the fraction of the 4-coordinated cross-links, $\tilde{n}_X(\tilde{l}_0)$, strongly modulates the initial shear modulus of networks of low to moderate connectivities, while for networks of very high connectivity the dependence on connectivity weakens and becomes less significant. Note that by construction, the scaling relations (4.2) or (4.4) tend to underestimate the G_0 at very small network connectivities ($\tilde{n}_X < 0.1$), as they predict $G_0 \to 0$ for vanishingly small $\tilde{n}_X$, despite

the fact that G_0 will have a small nonzero value at the geometric percolation limit.

4.3 Comparison with experiments

By combining equations (4.4), (3.11), (3.9) and (3.2) it is now possible to predict the initial elastic shear modulus G_0 for any RCL network just by knowing the macroscopic parameters: the concentration of filaments c_f, the concentration of cross-linking molecules c_cp and filament length l_0.

In order to demonstrate the quality of scaling relation (4.4) in predicting the initial shear modulus of a network, Figure 4.2a shows a comparison between the measured G_0 of isotropically cross-linked F-actin/rigor-HMM networks (Tharmann et al., 2007; Lieleg et al., 2009a) as a function of the concentration ratio $r_\mathrm{ac} = c_\mathrm{f}/c_\mathrm{cp}$, and predictions calculated on the basis of expression (4.4). The results in Figure 4.2a are calculated for pre-factor $A \approx 28$ and with the remaining parameters obtained as follows: l_c is solved numerically from expression (3.11) for known c_f, c_cp, l_0, as was done in Figure 3.4; $\tilde{n}_\mathrm{X}$ is obtained from (3.2) and ξ from (3.9).

Remarkably, in Figure 4.2a it can be seen that, for networks with $c_\mathrm{f} = 9.5\,\mu$M (blue) or $c_\mathrm{f} = 14.3\,\mu$M (green), the agreement with the experimentally measured G_0 is excellent over a wide range of r_ac, without any adjustments of the model parameters. Only for $r_\mathrm{ac} \gg 1$, when the networks are approaching the low-connected L-only limit, G_0 is expected to be underestimated due to the limitations of the expression (4.4), as discussed above (see Figure 4.1c). This is necessarily not a disadvantage, because at low cross-link concentrations ($r_\mathrm{ac} > 1000$), the F-actin/rigor-HMM network modulus becomes indistinguishable from that of entangled actin gels. (Luan et al., 2008).

In contrast, at larger filament concentrations, namely $c_\mathrm{f} = 19\,\mu$M (red) and $c_\mathrm{f} = 23.8\,\mu$M (black), the expression (4.4) significantly underestimates the experimental data over the entire range of r_ac. By allowing the proportionality constant in (4.4) to be a free parameter of the model, the experimental data for larger c_f show trends that can be fitted by the expression

$$G_0 = A^* \frac{\kappa}{l_\mathrm{c}^4} \left(\frac{l_\mathrm{c}}{\xi}\right)^3 \left(\frac{\tilde{l}_0 - 3}{\tilde{l}_0 - 1}\right)^5 , \tag{4.5}$$

as seen in Figure 4.2b. However, the fitting pre-factor A^* in (4.5) is found to be ~ 1.7 to ~ 2.5 times larger than what is expected from the original model, e.g. $A^* \approx 50$ for $c_\mathrm{f} = 19\,\mu$M (red dotted line) and $A^* \approx 72$ for $c_\mathrm{f} = 23.8\,\mu$M (black solid line). Although the bending stiffness of F-actins in the presence of HMM

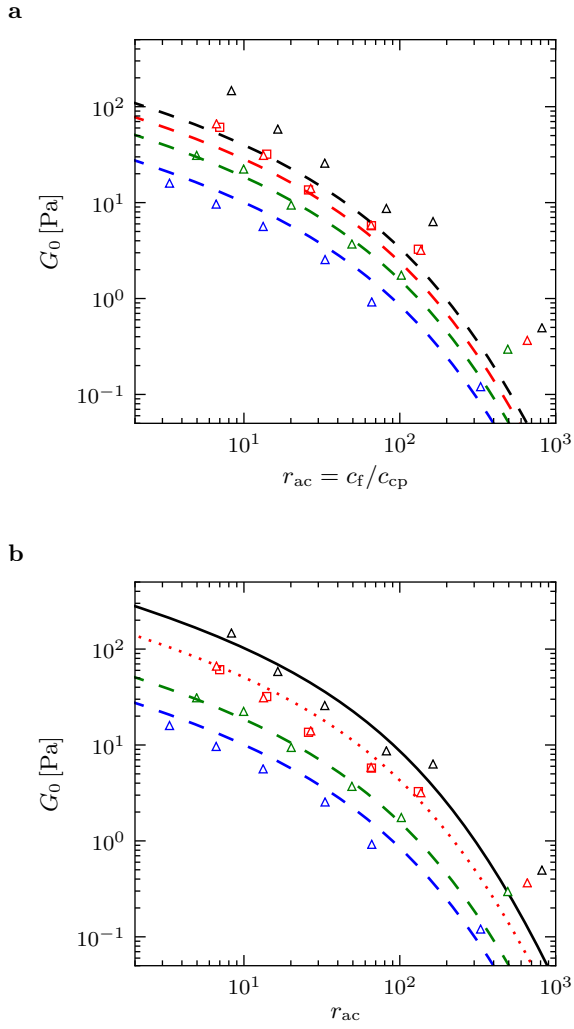

Figure 4.2. Small strain behavior of F-actin/rigor-HMM networks. The initial elastic shear modulus G_0 as a function of filament/cross-link concentration ratio $r_{ac} = c_f/c_{cp}$ for F-actin length $l_0 = 21\,\mu$m and actin concentrations: c_f [μM]: 9.5 (blue), 14.3 (green), 19 (red) and 23.8 (black). The measurements are obtained from Tharmann et al. (2007) (△) and Lieleg et al. (2009a) (□). Lines correspond to predictions according to (4.4) with pre-factor A: ≈ 28 (dashed), ≈ 50 (dotted) and ≈ 72 (solid).

molecules can be somewhat larger than what was used for calculations in Figure 4.2 (Oosawa, 1980), this alone cannot explain the surprising disparity observed for G_0 at increased c_f. In the remainder of this section we discuss some features of F-actin/rigor-HMM networks that might explain the unexpectedly large G_0 observed for high c_f in Figure 4.2b.

4.3.1 Interactions between decorating HMM molecules

Unlike many other actin binding proteins, which tend to bundle F-actins already at moderate concentrations (Lieleg et al., 2010), rigor-HMMs organize F-actins specifically into the isotropically cross-linked networks at any concentration (Tharmann et al., 2007). This unique organizational ability of HMM molecules, despite being poorly understood, is likely to originate from their structure.

HMM is a fragment of myosin II motor protein produced by fast trypsin or chymotrypsin digestion. In terms of molecular mass, 405 kDa HMM (Young et al., 1965) is a rather heavy F-actin cross-linking protein, when compared to 56 kDa fascin, 102 kDa scruin (Schmid et al., 1994; Way et al., 1995) or up to 280 kDa vertebrate filamins (Stossel et al., 2001). Because the proteolytic enzyme sensitive region in myosin is located some $600-900$ Å away from the actin binding domains (myosin heads), each HMM molecule, in addition to the two globular head domains, contains a rod-like coiled-coil domain up to 900 Å long; this is often termed subfragment 2 or S2 (Young et al., 1965; Sellers, 2000).

In physiological conditions, the S2 fragments have the tendency to self-associate (Sutoh et al., 1978). HMMs can bind F-actins up to stoichiometric ratio of 1 HMM molecule per 1 actin monomer (Rizzino et al., 1970), which suggests that F-actins in the network can be substantially decorated by HMMs. Since the structure of decorated F-actins is such that HMM S2 rod domains are sticking into the solvent, the effective diameter of a HMM decorated F-actin can reach $\sim 0.18\,\mu$m, i.e. ~ 25 times as large as the native actin diameter. For networks with low actin concentration this relatively large excluded volume around the decorated F-actins is less relevant, since the mesh size of the network is even larger; the mesh size ξ according to (3.9)[1] for $c_\mathrm{f} = 14\,\mu$M is of order of $\sim 0.3\,\mu$m. However, for larger c_f, in particular, for networks $c_\mathrm{f} = 19\,\mu$M and $c_\mathrm{f} = 23.8\,\mu$M in Figure 4.2, the mesh size is of order of ~ 0.25 and $\sim 0.22\,\mu$m, respectively. Because small mesh size is expected to increase molecular crowding of decorating HMMs around the cross-linking sites and in between the filaments, it is probable that HMMs in the volume overlapping regions interact through their S2 domains, as recently suggested by F-actin motility

[1] For F-actin, the concentration $24\,\mu\mathrm{M} = 1\,\mathrm{mg/ml}$.

assays with HMM motors attached to an SiO_2 substrate (Persson et al., 2010). Such interactions then, could additionally increase the network stiffness.

4.3.2 Steric filament effects

An alternative explanation for the discrepancy of G_0 at higher c_f might be that the expression (4.4) is not accounting for the steric hindrance between filaments, which incidentally are also not considered in the network generation method (see § 2.2). However, the steric effects, generally, could be particularly interesting at higher filament concentration, since it is known that they could cause jamming (Philipse, 1996).

If present, the steric interactions between filaments would not just increase the total number of filament constraints in the network, but, at the same time, would reduce the length l_c. Note that steric hindrance is meaningful only if filaments intend to cross-over each other. Up to first approximation and for small strains, these constraints can be seen as extra cross-links of X-type. Thus, rather than changing the behavior captured by expressions (4.4) or (3.11), it is reasonable to expect that steric interactions would mainly affect the connectivity $\tilde{n}_X$ by adding a c_f-dependent fraction of extra contacts between filaments in the network. Assuming that (extra) steric contacts contribute to $\tilde{n}_X$, the sensitivity of G_0 on sterically enhanced connectivity can be easily demonstrated by using expressions (3.2) and (4.2), e.g. for a network at moderate connectivity, taken as a reference, with $\tilde{n}_X \approx 0.51$ (corresponding to $\tilde{l}_0 \approx 8$), $l_0 = 21\,\mu$m and $l_c \approx 2.6\,\mu$m.

Assuming two extra constraints per filament due to steric hindrance, then $\tilde{l}_0 \rightsquigarrow 10$, thereby increasing the effective connectivity, $\tilde{n}_X \rightsquigarrow 0.60$, and decreasing the effective mean section length, $l_c \rightsquigarrow 2.1\,\mu$m, so that the initial modulus G_0 becomes a factor of ~ 1.9 higher than in the reference network. For three steric contacts per filament, $\tilde{l}_0 \rightsquigarrow 11$, $\tilde{n}_X \rightsquigarrow 0.64$, $l_c \rightsquigarrow 1.9\,\mu$m and the initial shear modulus increases by a factor of ~ 2.5. The enhancement of the modulus by a relatively small correction of the connectivity due to steric contacts between filaments might therefore explain the discrepancy observed in Figure 4.1.

4.4 Dependence on concentration

The dependence of the small strain network response on filament (c_f) and cross-linking molecule (c_{cp}) concentrations is especially interesting from the practical point of view, since this information is easily accessible in experiments. Generally, this dependence is presented in a form of scaling, $G_0 \propto {c_f}^x {c_{cp}}^y$, where the exponents x and y are $\approx 1 - 2.5$ (MacKintosh et al., 1995; Satcher and Dewey,

1996; Gardel et al., 2004a; Luan et al., 2008; Lin et al., 2010b) and $\approx 0.1 - 1.5$ (Wagner et al., 2006; Luan et al., 2008; Lieleg et al., 2007), respectively. In particular, the exponents commonly reported for isotropically cross-linked networks are: $x \approx 2 - 2.5$ and $y \approx 0.6 - 1.2$ (Tharmann et al., 2007; Luan et al., 2008; Lin et al., 2010b).

In the limit of high concentrations and high connectivity it is expected that the mesh size becomes equal to the mean section length, $l_c \approx \xi$. Using this, the scaling given by expression (4.2) reduces to $G_0 \propto (\kappa/\xi^4)\tilde{n}_X^{2.5}$. Since it follows from expression (3.9), that $(t/\xi)^2 \propto c_f/\rho_f$ for network with constant connectivity, the initial modulus of such networks scales with filament concentration as $G_0 \propto c_f^2$ (Satcher and Dewey, 1996). This quadratic dependence of initial shear modulus on filament concentration is typical for foams (Gibson and Ashby, 1997), that on average, have connectivity of 4 independent on density (only the struts get a different aspect ratio t/ξ) which enters the scaling law as the proportionality factor between $G_0 l_c^4/\kappa$ and $(l_c/\xi)^2$.

Generally however, the dependence of the initial shear modulus on concentrations of constituents for our network model is not a trivial power law because the initial modulus in (4.2) and the mesh size in (3.9) are both nonlinear functions of the topological parameter $\tilde{l}_0 = l_0/l_c$, as can be seen in Figure 4.1. By combining expressions (3.9), (3.12) and (4.2), the initial modulus of the networks, for particular type of filaments and cross-linking molecules, can be written as

$$G_0 \propto l_0^{-2/3}\, c_{cp}^{1/3}\, c_f^{7/6}\, \tilde{n}_X^{2.5}(1 - \tilde{n}_L)^{3/2}, \tag{4.6}$$

but the topological functions $\tilde{n}_X$ and $\tilde{n}_L$, through l_c and equation (3.12), still depend on l_0, c_f and c_{cp}. For networks of constant l_0 and constant connectivity $\tilde{n}_X$, however, the dependence of G_0 on constituent concentrations from (4.6) can be expressed in a relatively simple way.

Since for constant l_0 and $\tilde{n}_X$ from (3.2) follows that l_c is also a constant, form (3.12) we obtain the condition that the concentration of filaments and cross-linking molecules are proportional to each other, $c_f \propto c_{cp}$. This condition simply suggests that, for constant l_0, constant connectivity of the network can be maintained by keeping the ratio $c_f/c_{cp} =$ constant, which could be an interesting insight for the experiments where the connectivity, in principle, is not measurable. For constant l_0 and $\tilde{n}_X$ then, the scaling relation (4.6) reduces to $G_0 \propto {c_{cp}}^{1/3}\, {c_f}^{7/6}$, which with $c_f \propto c_{cp}$ gives either $G_0 \propto {c_f}^{3/2}$ or $G_0 \propto {c_{cp}}^{3/2}$. Note that the individual exponents, $x = 3/2$ or $y = 3/2$, can not be directly compared to those reported in above experiments, since in those experiments condition of constant network connectivity is not strictly maintained.

4.5 Conclusions

The complete scaling of the initial stiffness G_0 of rigidly cross-linked networks comprises two contributions: (1) general scaling characteristics for bending structures and (2) dependence on topology, amongst which the distribution of cross-links over three cross-link types.

It was found that topological effects on the small–strain behavior can be captured by a power-law dependence on two dimensionless numbers, that are of geometrical and topological nature. An increase in the number of X cross-links enhances the connectivity of the network structure, thus resulting in a higher shear modulus. Although the relative number of X cross-links is a very well identified measure in numerical studies, it cannot easily be obtained from experiments.

F-actin/rigor-HMM networks have been suggested as a possible model system for the experimental study of the small strain mechanics of isotropically cross-linked biopolymer networks in the limit of rigid cross-links (Tharmann et al., 2007). When compared to the experimental results for such F-actin/rigor-HMM networks, the scaling relation in (4.4) predicts rather well the initial shear modulus G_0 of networks with actin concentrations up to $c_\mathrm{a} = 14.3\,\mu$M over the whole range of HMM concentrations. However, for larger actin concentrations, the equation (4.4) is significantly underestimating G_0. This discrepancy in G_0 found for higher actin concentration is suggesting that there might be additional features present in the network which enhance the network stiffness. However, it remains unclear if this enhancement is general and significant for all isotropically cross-linked networks via steric hindrance between the filaments or if it is a feature specific for the F-actin networks when cross-linked by rigor-HMM.